Role of Long-Range Repulsive Interactions in Two-Dimensional Colloidal Aggregation: Experiments and Simulations

A. Moncho-Jordá,† F. Martínez-López,† A. E. González,‡ and R. Hidalgo-Álvarez*,†

Biocolloid and Fluid Physics Group, Department of Applied Physics, Granada University, Granada 18071, Spain, and Center for Physical Sciences, National Autonomous University of Mexico, Apartado Postal 48-3, 62251 Cuernavaca, Mexico

Received April 30, 2002. In Final Form: August 23, 2002

A theoretical model for the interaction between colloidal particles trapped at the air−water interface is proposed in order to explain experimental aggregation results. Kinetic and structural aspects of 2D aggregation processes point out the long-range nature of the particle interactions. These interactions have been modeled by means of monopolar and dipolar repulsive forces, which depend on the monopole and dipole surface fractions at the emergent part of the colloidal particles, f_{mon} and f_{dip}, respectively. Brownian dynamics simulations have been used to fit the model to experiment results using the fractal dimension d_f and the kinetics exponent z as comparative parameters. Simulation results show that dipolar interaction controls aggregation at high subphase salt concentration whereas the monopolar interaction determines aggregation at low salt concentrations. Moreover, results show that f_{mon} is the main parameter controlling kinetics in 2D aggregation and, hence, a critical coagulation concentration (CCC) can be defined from the salt concentration at which the monopole fraction becomes zero, $f_{mon} = 0$.

1. Introduction

Aggregation processes are of fundamental importance in a wide variety of natural systems and industrial applications such as aerosols, droplet formation, production of polymers, paints, and biological materials.[1,2,3] The colloidal suspension features (particle size, surface charge density, particle density, hydrophobic/hydrophilic character, etc.) and the existence of external fields are important factors determining stability and/or aggregation kinetics, but confinement effects must also be taken into account.[4]

Recently, the behavior of colloidal dispersions confined in a 2D geometry has drawn wide interest. From an experimental point of view, there are different forms to obtain 2D systems. For example, a dispersion of charged particles bounded by two charged plates of the same sign constitutes a 2D system since the electrostatic repulsion makes the particles remain confined at the intermediate plane between two walls.[5,6] Also, a system consisting of particles trapped at the air−liquid or liquid−liquid interfaces can be considered to be a 2D system. The formation of monolayers is especially interesting because of the ability of particles to affect the stability of emulsions, foams, and interfacial properties.

Pieranski did the first study on 2D colloidal dispersions,[7] and reported a system of polystyrene latex particles trapped at the air−water interface. He observed the formation of 2D colloidal crystals and suggested that this ordered phase was a consequence of strong dipole−dipole interactions. This interaction is responsible for the nonisotropic forces between clusters formed in aggregation processes and gives an explanation for the low fractal dimensions observed by Hurd and Schaefer in the aggregation of silica microspheres at the air−water interface.[8]

Robinson and Earnshaw studied the colloidal aggregation of a similar system. To explain the large stability of colloidal monolayers observed even for very high salt concentrations, they also proposed the existence of dipole−dipole repulsive interactions.[9] According to them, the dipoles are surface charges at the top of the particle that have trapped a counterion from the solvent during the initial turbulent spreading. Curiously, William and Berg observed that colloidal dispersions at the air−water interface were more unstable than in solution.[10] This apparent contradiction between both sets of experimental results could be explained by the different methods used to form the monolayer of particles.

The study of interfacial aggregation has also been achieved using large particles with a size of around 70 micrometers, which are not sensitive to the Brownian motion. In these conditions, the aggregation process is controlled essentially by strong and long-ranged attractive capillary interactions and by hydrophobic/hydrophilic forces. For example, it has been found that the cluster fractal dimension decreases as particle hydrophobicity increases, being lower for hydrophobic particles due to restructuring of the inner cluster structures.[11−15]

* Corresponding author. E-mail: rhidalgo@ugr.es.
† Granada University.
‡ National Autonomous University of Mexico.

(1) Brown, W. D.; Ball, R. C. *Kinetics of Aggregation and Gelation*; North-Holland: Amsterdam, 1984.
(2) Sonntag, H.; Strenge, K. *Kinetics and Structure Formation*; Plenum Press: New York, 1987.
(3) Hidalgo-Álvarez, R.; Martín, A.; Fernández, A.; Bastos, D.; Martínez, F.; de las Nieves, F. J. *Adv. Colloid Interface Sci.* **1996**, *67*, 1.
(4) Crocker, J. C.; Grier, D. *Phys. Rev. Lett.* **1996**, *77*, 1897.
(5) Kepler, G. M.; Fraden, S. *Phys. Rev. Lett.* **1994**, *73*, 356.
(6) Carbajal-Tinoco, M. D.; Castro-Román, F.; Arauz-Lara, J. L. *Phys. Rev. E* **1996**, *53*, 3745.
(7) Pieranski, P. *Phys. Rev. Lett.* **1980**, *45*, 569.
(8) Hurd, J.; Schaefer, D. W. *Phys. Rev. Lett.* **1985**, *54*, 1043.
(9) Robinson, D. J.; Earnshaw, J. C. *Langmuir* **1993**, *9*, 1436.
(10) Williams, D. F.; Berg, J. C. *J. Colloid Interface Sci.* **1992**, *152*, 218.
(11) Hórvölgyi, Z.; Medveczky, G.; Zrínyi, M. *Colloids Surf.* **1991**, *60*, 79.
(12) Hórvölgyi, Z.; Medveczky, G.; Zrınyi, M. *Colloid Polym. Sci.* **1993**, *271*, 396.

10.1021/la0258805 CCC: $22.00
Published on Web 10/26/2002

Recent experimental results showed that 2D-structured colloidal dispersion formed at the air−water and oil−water interfaces cannot be explained only by considering dipolar repulsive interactions; therefore, a longer-range interaction potential is necessary.[16] Quesada et al.[17] carried out experiments on stable colloidal monolayers at the air−water interface, and they showed that the particle interaction potential manifests a long-ranged repulsive barrier (close to 7 times the particle diameter). In that study, they also suggested the possibility of Coulombic electrostatic forces (i.e., monopolar forces) as well as dipolar ones. The existence of long-ranged repulsive forces was also suggested by Moncho et al.[18] in aggregation experiments at the air−salt solution interface for different salt concentrations and different counterion valences, where the critical coagulation concentration (CCC) was estimated to be 1 order of magnitude larger than in bulk solution.

Theoretically, Hurd[19] studied the interactions between charged particles at the interface using a model developed by Stillinger.[20] Terao and Nakayama[21] studied the crystallization of 2D colloidal systems by means of Monte Carlo simulations. Martínez et al.[22] developed a theoretical model for the particle interactions at the air−aqueous solution interface that considers the DLVO (repulsive double-layer interactions between the immersed parts of the particles and van der Waals forces between both immersed and emergent parts separately), capillary, and hydrophobic interactions in addition to the dipole−dipole repulsive interactions between nonimmersed parts of the colloidal particles. Recently, Sun and Stirner[23] used molecular dynamics to show that the long-range repulsive interactions between particles at the oil−water interface is principally caused by monopole−monopole Coulombic interactions.

This work aims to study colloidal interaction since those are key issues in determining kinetic and structural aspects of aggregation. According to previous experimental results, colloidal stability and aggregation at the air−water interface are controlled by long-range repulsive interactions. Thus, in this paper, we intend first to study how long-range interactions affect coagulation of polystyrene latex particles dispersed at the air−salt solution interface and then to present a theoretical model for the particle interaction potential capable of explaining kinetic and structural properties of the aggregation. In this model, long-range interactions are accounted for by means of two different interactions: (i) dipole−dipole forces that control the aggregation at high ionic strength and (ii) monopole−monopole Coulombic interactions that govern stability at salt concentrations lower than the CCC. The experimental results are compared to theoretical predictions through Brownian dynamics simulations.

This paper is organized as follows. In section 2, the most important properties of the aggregation process are reviewed, and our theoretical model is presented. In section 3, experiments are briefly described, and simulation methods are explained. Section 4 deals with comparisons between theory and experiments. Finally, section 5 summarizes the results and reaches some conclusions.

2. Theoretical Background

2.1. Aggregation Kinetics and Cluster Fractal Dimension. Kinetic and structural features of aggregation have been studied numerically using the cluster size distribution $n_i(t)$, number of clusters of size i at time t, and the cluster fractal dimension d_f, respectively.

On one hand, the kinetics can be characterized as a whole using the long-time behavior of the weight-average cluster size

$$S_w(t) = \sum_i i^2 n_i(t) / \sum_i i n_i(t) \approx t^z \qquad (1)$$

where z, the so-called kinetic exponent,[24] is closely related to cluster reactivity, higher z values corresponding to more-reactive large clusters in comparison with small ones.

On the other hand, the fractal dimension of the inner structure of clusters can be obtained from the relation between their radius of gyration, R_g, and their size i:[25]

$$R_g \approx i^{-1/d_f} \qquad i \gg 1 \qquad (2)$$

Both parameters, z and d_f, are dependent on the main features of the particle−particle interaction potential. Generally, this interaction is attractive for short particle−particle separation distances but repulsive for moderate and large distances and has the form of a repulsive barrier. In fact, it has been demonstrated by simulation that growth of the repulsive barrier height, which is equivalent to a decrease in the sticking probability, increases both the kinetic exponent z and the fractal dimension.[26,27]

However, aggregation is affected not only by the repulsive barrier height but also by its width. Since for forces with a long enough repulsive range all particles belonging to two neighboring clusters repel each other, the total repulsion between two large clusters is higher than that between small ones because of the superposition of all pairwise particle−particle interactions. Hence, a long-range repulsive interaction makes big clusters less reactive than small ones, and it is expected that

$$z_{\text{long range}} < z_{\text{short range}} \qquad (3)$$

Moreover, long-range repulsions between clusters make it difficult for them to approach close enough to interpenetrate deeply, being that aggregation is mainly favored at the tips, leading to the formation of more linear clusters with a lower fractal dimension.

2.2. Interaction Potential. Achieving an expression for the particle−particle interaction potential between charged spherical beads trapped at the air−water interface has additional complexities in comparison to that of bulk solutions. For instance, the interaction depends on the contact angle close to $\theta = 82$ degrees for polystyrene latex beads determining the particle position at the interface and its immersed fraction. In addition, there are new forces that do not appear in 3D dispersions, as the above-

(13) Hórvölgyi, Z.; Németh, S.; Fendler, J. H. *Colloids Surf., A* **1993**, *71*, 327.
(14) Hórvölgyi, Z.; Máté, M.; Zrınyi, M. *Colloids Surf. A* **1994**, *84*, 207.
(15) Vincze, A.; Fata, R.; Zrínyi, M. *J. Chem. Phys.* **1997**, *107*, 7451.
(16) Aveyard, R.; Clint, J. H.; Nees, D.; Paunov, V. N. *Langmuir* **2000**, *16*, 1969.
(17) Quesada-Pérez, M.; Moncho-Jordá, A.; Martínez-López, F.; Hidalgo-Álvarez, R. *J. Chem. Phys.* **2001**, *115*, 10897.
(18) Moncho-Jordá, A.; Martínez-López, F.; Hidalgo-Álvarez, R. *J. Colloid Interface Sci.* **2002**, *249*, 405.
(19) Hurd, A. J. *J. Phys. A: Math. Gen.* **1985**, *18*, L1055.
(20) Stillinger, F. H. *J. Chem. Phys.* **1961**, *35*, 1584.
(21) Terao, T.; Nakayama, T. *Phys. Rev. E* **1999**, *60*, 7157.
(22) Martínez-López, F.; Cabrerizo-Vílchez, M. A.; Hidalgo-Álvarez, R. *J. Colloid Interface Sci.* **2000**, *232*, 303.
(23) Sun, J.; Stirner, T. *Langmuir* **2001**, *17*, 3103.
(24) Meakin, P.; Vicsek, T.; Family, F. *Phys. Rev. Lett.* **1985**, *31*, 564.
(25) Vicsek, T. *Fractal Growth Phenomena*; World Scientific: Singapore, 1992.
(26) González, A. E. *Phys. Rev. Lett.* **1993**, *71*, 2248.
(27) Moncho-Jordá, A.; Odriozola, G.; Martínez-López, F.; Schmitt, A.; Hidalgo-Álvarez, R. *Eur. Phys. J. E* **2001**, *50*, 471.

mentioned repulsive dipolar interaction and also capillarity attractive forces.[28]

To simplify the calculation of the different interaction potential terms, two approximations have been made. First, the interaction between particles at the interface is assumed to occur between their emergent and immersed parts separately, and there is no interaction between the emergent and immersed parts of different particles. Second, the interfacial meniscus is flat near the particle surface. Last, the approximation is justified because of the very small Bond number value for the particle used in our experiments (735-nm diameter). The flat meniscus hypothesis also implies that, if the interaction superposition is verified, capillarity interaction is negligible even for large aggregates as a result of their noncompact fractal structure.

The proposed model considers the following contributions to the total energy: electrostatic interactions between double layers of the immersed colloidal particle parts, van der Waals interactions between immersed and emergent particle parts (with different Hamaker constants), and short-range attractive hydrophobic interaction between immersed parts. Additionally we will consider three interactions involving only the emergent particle surface: dipole−dipole, monopole−monopole and monopole−dipole repulsive interactions. Thus, the total pairwise interaction potential reads as

$$V_T = V_e + V_{vdW} + V_{hydro} + V_{dip-dip} + V_{mon-mon} + V_{mon-dip} \quad (4)$$

Because of their short range, double layer, hydrophobic, and the London−van der Waals interactions can be calculated using the Derjaguin approximation, which allows one to determine the interaction between two spherical particles separated a minimum distance h_0 as

$$V(h_0) = \int V^{(flat)}(h)\, dS(h) \quad (5)$$

where $V^{(flat)}(h)$ is the interaction potential between flat half spaces per unit of area and h is the local distance between the elementary rings with area $dS(h)$ dividing the particle surface. So, to compute the double layer, hydrophobic, and London−van der Waals interactions, expressions must be given for their interactions between half spaces.

The electrostatic interaction potential per unit of area for half spaces separated a distance h is given by[35]

$$V_e^{(flat)}(h) = 64 n^0 k_B T Z^2 \kappa^{-1} \exp(-\kappa h) \quad (6)$$

where $Z = \tanh(ze\psi_0/4k_BT)$, n^0 is the salt concentration, k_B is the Boltzmann constant, T is the temperature, e is the electron charge, κ^{-1} is the Debye length, z is the ionic valence, and ψ_0 is the surface potential, which for a 1:1 electrolyte may be obtained from the expression[36]

$$\sigma_0 = \frac{2\epsilon_r\epsilon_0\kappa k_B T}{e} \sinh\left(\frac{e\psi_0}{2k_B T}\right) \quad (7)$$

where σ_0 is the experimentally determined surface charge density that depends on the pH of the experiment.

Analogously, the van der Waals interaction energy per unit of area between half spaces separated a distance h is given by[37]

$$V_{vdW}^{(flat)}(h) = \begin{cases} -\dfrac{A_{air}}{12\pi h^2}(1 + bh/\lambda)^{-1} & \text{emergent parts} \\ -\dfrac{A_{water}}{12\pi h^2}(1 + bh/\lambda)^{-1} & \text{immersed parts} \end{cases} \quad (8)$$

where $b = 5.32$, $\lambda = 100$ nm, and constants $A_{air} = 6.6\times10^{-20}$ J and $A_{water} = 0.95\times10^{-20}$ J are the Hamaker constants for the polystyrene−polystyrene interaction in air and in water, respectively.

Finally, the hydrophobic energy between two plates is given by[38]

$$V_{hydro}^{(flat)}(h) = \begin{cases} 0 & \text{emergent parts} \\ W_0 e^{-h/\lambda_0} & \text{immersed parts} \end{cases} \quad (9)$$

where $W_0 = -6 \times 10^{-2}$ J m^{-2} determines the interaction strength and $\lambda_0 = 1.6 \times 10^{-9}$ m, its range.[39] For a more complete analysis of these interaction potential terms, we refer the reader to Martınez et al.[22]

The remaining three interaction terms in eq 4, $V_{dip-dip}$, $V_{mon-mon}$, and $V_{mon-dip}$ originate directly from the surface groups at the particle surface part above the liquid interface (i.e., at the air phase). These interactions are large and long-ranged because of the absence of a screening counterion cloud. The chemical surface groups of the air-exposed particle part can be found in three different forms: nondissociated, dissociated, and forming dipoles. The nondissociated groups will be the most common configuration and they do not contribute to the interaction. On the contrary, if the external surface groups are dissociated, they interact through the air phase with an interaction potential of the form $V(r) \approx 1/r$. Alternatively, a surface group can appear, forming an electric dipole together with a counterion adsorbed from the subphase. Both ions have opposite charge, and the distance separating them is close to the effective diameter of the trapped counterion, $d \approx 0.3$ nm for the Br^- case. These dipoles generate a strong dipolar field with a significant long range, whose potential dependence on distance r is $V(r) \approx 1/r^3$.

The main question that arises from the previous analysis is, How do monopoles and dipoles originate? A plausible explanation was suggested by Robinson and Earnshaw in 1993[9] and was supported later by Sun and Stirner.[23] The particle monolayer is formed from a drop sample of particles using methanol as a spreading agent. These particles have a small fraction of dissociated groups that during the turbulent spreading process are put in contact with the salty solution. Because of the subphase counterions' reach and the strength of the interaction between

(28) Chan, D. Y. C.; Henry J. R.; White, L. R *J. Colloid Interface Sci.* **1981**, *79*, 410.
(29) Robinson, D. J.; Earnshaw, J. C. *Phys. Rev. A* **1992**, *46*, 2045.
(30) Dhont, J. K. G. *An Introduction to the Dynamics of Colloids*; Elsevier: New York, 1996.
(31) Risken, H. *The Fokker−Planck Equation: Methods of Solution and Applications*; Springer-Verlag: 1989.
(32) Press, W. H.; Teukolsky, S. A.; Vetterling, W. T.; Flannery, B. P. *Numerical Recipes in C*; Cambridge University Press: Cambridge, U.K.,1995.
(33) Rhee, Y.-J.; Halley, J. W.; Hautman, J.; Rahman, A. *Phys. Rev. B* **1989**, *40*, 36.
(34) Lekner, J. *Physica A* **1991**, *176*, 485.
(35) Verwey, E. J. W.; Overbeek, J. Th. G. *Theory of Stability of Lyophobic Colloids*; Elsevier: Amsterdam, 1948.
(36) Ohshima, H.; Furusawa, K. *Electrical Phenomena at Interfaces*; Marcel Dekker: 1998.
(37) Gregory, J. *J. Colloid Interface Sci.* **1981**, *83*, 138.
(38) Christenson, H. K.; Claesson, P. M. *Science (Washington, D.C.)* **1988**, *239*, 390.
(39) Israelachvili, J. *Intermolecular and Surfaces Forces*; Academic Press: New York, 1992.

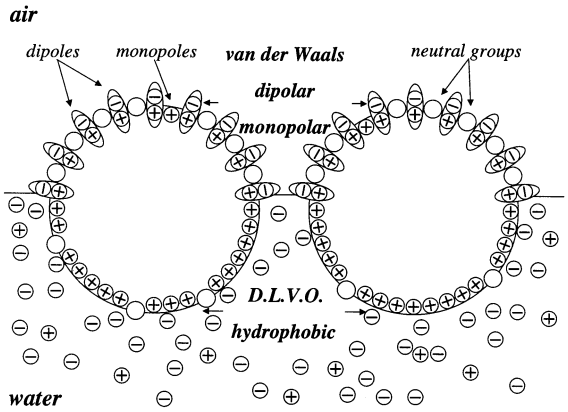

Figure 1. Sketch of particle arrangement at the air−water solution interface. The immersed parts interact through DLVO and hydrophobic forces and the emergent parts through van der Waals, dipolar, and monopolar interactions.

the counterions and the dissociated particle groups, it is expected that most of them can trap a counterion, forming a dipole that could be exposed to the air phase. The rest of the dissociated groups that do not form dipoles will stay as monopoles. Furthermore, as most of the dissociated species give rise to a dipole, it is expected that their fraction f_{dip} in relation to the total surface group was almost constant. The monopole fraction f_{mon} in relation to the total surface groups could increases when the subphase salt concentration decreases, as the counterion trapping probability also slightly decreases. As the number of initially dissociated chemical surface groups is small, most of them will be neutral (see Figure 1), being expected that

$$f_{mon}, f_{dip} \ll 1 \tag{10}$$

To estimate the monopolar, dipolar, and monopole−dipole interactions, monopoles and dipoles are expected to be homogeneously distributed over the emergent part of the particle. Thus, the pair interaction energy can be calculated by integrating numerically over the emergent parts of the two interacting particle surfaces S_1 and S_2:

$$V(h_0) = \int_{S_1}\int_{S_2} V(h)\, dS_1\, dS_2 = a^4 \int \sin\theta_1\, d\theta_1 \int d\phi_1 \int \sin\theta_2\, d\theta_2 \int d\phi_2\, U(\theta_1, \theta_2, \phi_1, \phi_2) \tag{11}$$

Here, a is the particle radius, $\theta_1, \phi_1, \theta_2$, and ϕ_2 are spherical coordinates in each particle center, and U contains all monopole−monopole, monopole−dipole, and dipole−dipole contributions:

$$U = \frac{\sigma_0^2}{4\pi\epsilon\epsilon_0}\left\{ f_{mon}^2\left(\frac{1}{F(a,a)}\right) + f_{mon} f_{dip}\left(\frac{2}{F(a,a)} - \frac{1}{F(a+d,a)} - \frac{1}{F(a+,a+d)}\right) + f_{dip}^2\left(\frac{1}{F(a,a)} - \frac{1}{F(a+d,a)} - \frac{1}{F(a,a+d)} + \frac{1}{F(a+d,a+d)}\right)\right\} \tag{12}$$

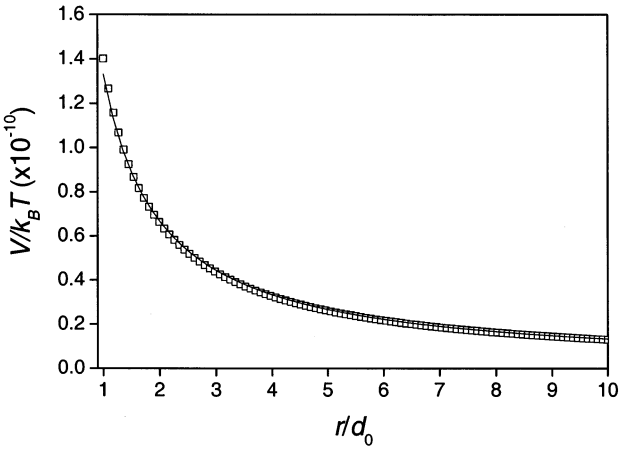

Figure 2. Comparison between the exact calculation of the monopolar interaction between two homogeneously charged particle surfaces (□) and the Coulombic approximation for large distance (—). d_0 indicates the particle diameter. The fitting between the exact and approximated data gives a fitting constant of $k_1 = 3.97 \times 10^{-17}$ J m.

where d is the dipole length, $F(A, B) = \sqrt{X^2+Y^2+Z^2}$ and

$$X = A\sin\theta_1\cos\phi_1 - B\sin\theta_2\cos\phi_2 - 2a - h_0$$
$$Y = A\sin\theta_1\sin\phi_1 - B\sin\theta_2\sin\phi_2$$
$$Z = A\cos\theta_1 - B\cos\theta_2 \tag{13}$$

For a complete analysis of last term, which corresponds to the dipole−dipole interaction energy $V_{dip-dip}$, we again refer the reader to Martınez et al.[22] Here, just two terms involving monopoles will be analyzed. Let us consider first the monopole−monopole interaction energy $V_{mon-mon}$. Figure 2 shows this monopolar interaction energy for particles with radius $a = 735$ nm, surface charge density $\sigma_0 = 0.09$ C m^{-2}, and contact angle $\theta = 82°$ at $T = 293$ K and $f_{mon} = 1$. A decrease of the interaction energy with the inverse of distance between particles is evident for large distances. Figure 2 also shows data fitting to the theoretical limit for large distances:

$$V_{mon-mon}(r) = f_{mon}^2 k_1 \frac{1}{r}\; r \gg 1 \tag{14}$$

where k_1 is a constant that basically depends on particle surface charge density. Although our results show that eq 14 could be useful even at short distances, this is not a general property of all particle types. However, the dependence of interaction energy with the inverse of distance is a general result that is valid for charged systems and large enough distances, which is obtained as the first term from a mathematical expansion, the multipolar expansion, of the interaction energy.

If the multipolar expansion is carried out for the interaction between a charged system and a neutral one, the first nonnull term is given by

$$V_{mon-dip}(r) = k_2 \frac{\vec{P}\cdot\vec{r}}{r^3} \tag{15}$$

Here, vector $\vec{P}$ is the equivalent electric dipole of the neutral system, $\vec{r}$ is a vector indicating the relative position of both systems, and constant k_2 depends on the system's properties (charge distributions and charge amount). In our case, those systems are uniform distributions of monopoles and dipoles placed at the air-exposed part of

the particle surface. Thus, vector $\vec{P}$ is normal to the interface plane and vector $\vec{r}$ connects the particle centers, so both $\vec{r}$ and $\vec{P}$ vectors are always perpendicular, $\vec{P}\cdot\vec{r} = 0$, independent of the particle's relative position and the monopole−dipole interaction is zero in this approximation.

Hence, the interaction energy includes only four contributions: V_e, V_{vdW}, V_{hydro}, $V_{dip-dip}$ and $V_{mon-mon}$.

3. Materials and Methods

3.1. Experiments. Colloidal particles used in experiments were cationic polystyrene latex beads, which were prepared from styrene by free-emulsifier emulsion polymerization with azo *N*,*N*-dimethyleneisobutyramidine hydrocloride (AMBDA) as the initiator and NaCl as the buffer. The polymerization was carried out in a reactor fitted with a reflux condenser, stainless steel stirrer, and nitrogen inlet tube. The size distribution was determined by transmission electron microscopy. The average particle diameter was 735 ± 36 nm. The latex dispersion was cleaned first by serum replacement and second using a mixed-bed ion-exchange resin. Finally, a maximum surface charge density $\sigma_0 = 0.090 \pm 0.008$ C m^{-2} was determined by conductiometric titration.

Concerning the 2D colloidal dispersion, an aqueous KBr solution was introduced into a Teflon cell. Then, latex particles were deposited at the air−water interface using a microsyringe. The interface has to be as planar as possible to prevent the particle emigration as a consequence of gravity. The immersion of the latex beads into water was avoided by dispersing the particles using methanol as a spreading agent, according to the procedures described in refs 9 and 29. For this purpose, colloidal suspensions were prepared in a methanol solution and sonicated for five minutes to ensure a monodisperse sample. It should be noted that the use of methanol in the particle deposition is essential to obtaining a uniform monolayer. After methanol evaporation, the cell was covered with a thin glass plate to prevent contamination of the colloidal monolayer and convective fluxes produced by the air motion. Images of the interface were recorded with a digital camera (with 1280 × 1024 pixels) incorporated with a phase-contrast microscope. The magnification of the objective was fixed in such a way that the pixel diameter was as similar as possible to the particle size. Images were first acquired by a frame grabber and then transformed to binary images and analyzed to determine the average cluster size and the cluster fractal dimension. Furthermore, possible external vibrations were avoided by placing the system formed by the cell, microscope, and digital camera on an antivibratory table.

3.2. Simulations. The accuracy of the interaction potential model to explain aggregation experimental results has been analyzed using off-lattice Brownian dynamics simulations, which were carried out in a 2D square box with periodic boundary conditions.The motion of a colloidal particle (cluster) in a continuous medium is given by the Langevin equation, which in the diffusive time scale reads as[30]

$$\frac{d\vec{r}}{dt} = \frac{\vec{F}(t)}{\gamma} + \frac{\vec{f}(t)}{\gamma} \tag{16}$$

where $\vec{F}(t)$ is the total deterministic force acting on the particle (aggregate), $\vec{f}(t)$ is a random force due to its multiple collisions with environment molecules, and γ is the friction coefficient of the particle (aggregate) with the medium. Here, we assume that the Stokes law also applies to clusters and hence $\gamma = 6\pi\eta R_g$, where R_g is the cluster radius of gyration and η is the solvent viscosity. Although this is an approximation, corrections to it affect only the time scale and do not affect both the kinetic exponent z and the fractal dimension d_f.

The Langevin equation above has a corresponding Fokker−Plank equation for the probability $P(\vec{r}, t)$ of finding a cluster in position $\vec{r}$ at time t. This Fokker−Plank equation is given by[31]

$$\frac{\partial P}{\partial t} = \frac{1}{\gamma}\vec{F}\cdot\nabla_{\vec{r}}P + D\nabla^2_{\vec{r}}P \tag{17}$$

where $D = k_B T/\gamma$ is the cluster diffusion coefficient. The resolution of this equation in a 2D space together with initial conditions $P(\vec{r}, t = 0) = \delta(\vec{r} - \vec{r}_0)$ to obtain the cluster motion probability from $\vec{r}_0$ to $\vec{r}$ during time interval Δt leads to the multidimensional Gaussian distribution:

$$\begin{aligned} P(\vec{r}, \Delta t) &= \frac{1}{4\pi D\Delta t} e^{-|\vec{r}-\vec{r}_0-\vec{F}\Delta t/\gamma|^2/(4D\Delta t)} \\ &= \frac{1}{\sqrt{2\pi(2D\Delta t)}} e^{-1/2(x-x_0-F_x\Delta t/\gamma)^2/(2D\Delta t)} \\ &\times \frac{1}{\sqrt{2\pi(2D\Delta t)}} e^{-1/2(y-y_0-F_y\Delta t/\gamma)^2/(2D\Delta t)} \end{aligned} \tag{18}$$

Thus, the cluster relative displacement $\Delta x(= x - x_0)$ along the X axis during a time interval Δt is given by a Gaussian distribution with mean $\mu_X = F_x\Delta t/\gamma$ and variance $\sigma^2 = 2D\Delta t$; analogously, the cluster relative displacement $\Delta y(= y - y_0)$ along the Y axis during a time interval Δt is distributed as a Gaussian with mean $\mu_Y = F_y\Delta t/\gamma$ and the same variance, $\sigma^2 = 2D\Delta t$.

Brownian dynamics simulations of the aggregation were carried out using the above Gaussian distribution when moving aggregates randomly. However, some considerations must be taken into account to perform them adequately.

The above Gaussian distribution was obtained under the approximation of a constant and uniform deterministic force, so the simulation time interval Δt must be short enough to allow us to consider a force change negligible during the cluster movement. In our simulation, a time step $\Delta t = 3 \times 10^{-5}$ s was found to be adequate.

The distribution of random numbers generated during the simulation must approach as exactly as possible a Gaussian distribution, so we have used the Box−Muller method[32] to obtain a Gaussian distribution for a given μ and σ easily.

The mean aggregate displacement is dependent on the net force that other aggregates exert on it. This net force was computed under the assumption that particle interactions are additive (i.e., the total interaction between two clusters is the sum of all interaction forces between particles from one aggregate and those belonging to the other one).

The interaction force between particles can be determined by differentiation of the total pairwise interaction energy with respect to the interparticle distance r:

$$\vec{F} = -\frac{\partial V_T}{\partial r}\frac{\vec{r}}{r} = -\frac{\partial V'_T}{\partial r}\frac{\vec{r}}{r} + \vec{F}_{mon-mon} \tag{19}$$

where $V_T'(r)(= V_e(r) + V_{vdW}(r) + V_{hydro}(r) + V_{dip-dip}(r))$ and $\vec{F}_{mon-mon}$ represent the Coulombic force between monopoles. The four terms forming V_T' may be considered to be zero beyond a cutoff particle−particle distance, which depends on potential features. However, the long-range character of the Coulombic interactions makes it impossible to define any cutoff distance, and it must to be calculated separately. Moreover, the computation of the monopolar force that particle i feels due to particle j must be carried out by taking into account the different images of particle j on all periodic cells.[33,34]

$$\vec{F}_i \simeq f^2_{mon}k_1 \sum_{cells} \frac{\vec{r}_i - \vec{r}_j}{|\vec{r}_i - \vec{r}_j|^3} \tag{20}$$

where $k_1 = 3.97 \times 10^{-17}$ J m.

Defining dimensionless parameters $\xi = (x_i - x_j)/L$ and $\omega = (y_i - y_j)/L$ (where L is the size of the simulation box), the above expression can be rewritten as

$$\begin{aligned} F_x &= \frac{f^2_{mon}k_1}{L^2} \sum_{l=-\infty}^{\infty}\sum_{m=-\infty}^{\infty} \frac{\xi + l}{[(\xi + l)^2 + (\omega + m)^2)]^{3/2}} \\ F_y &= \frac{f^2_{mon}k_1}{L^2} \sum_{l=-\infty}^{\infty}\sum_{m=-\infty}^{\infty} \frac{\omega + m}{[(\xi + l)^2 + (\omega + m)^2)]^{3/2}} \end{aligned} \tag{21}$$

Since the sums in eq 21 are dimensionless quantities, they can

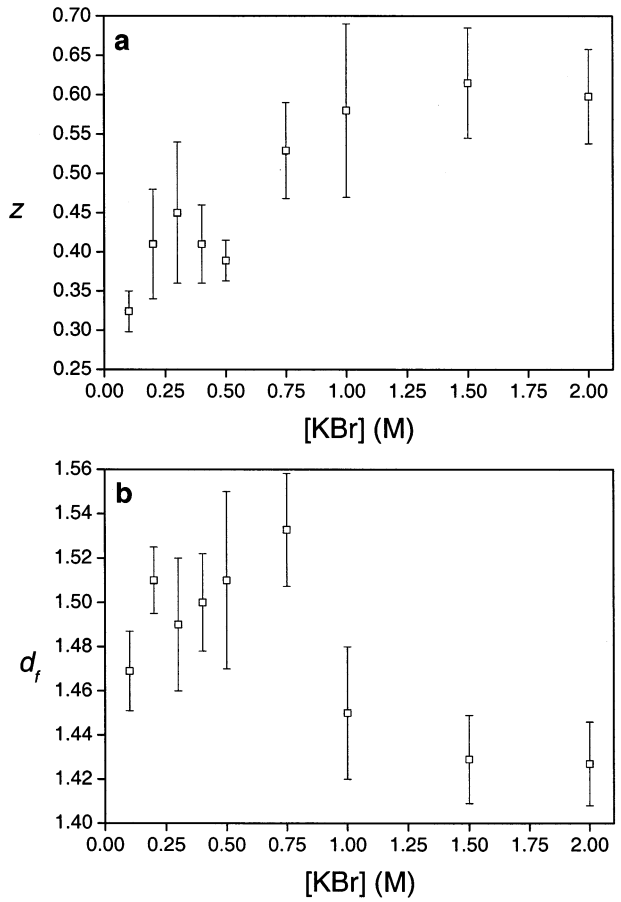

Figure 3. Kinetic exponent z (a) and cluster fractal dimension d_f (b) as a function of the subphase KBr concentration for all reported experiments. Above [KBr] = 1 M, both quantities reach constant values, $z \approx 0.6$ and $d_f \approx 1.435$.

be tabulated for later use in calculating the Coulombic forces between particles.

Finally, it should be noted that in carrying out a simulation, aggregation is considered to occur if a cluster overlaps another one. Then, the moved cluster position is corrected backward in the movement direction until only cluster surfaces remain in contact and both aggregates are joined irreversibly and moved as a new one.

4. Results and Discussion

To study the salt concentration effect on cluster structure and aggregation kinetics, experiments with different KBr solutions with concentration from 0.1 to 2 M were performed. All experimental temperatures and particle surface fractions were fixed to be 293 K and $\varphi = 0.04$, respectively.

Experimental results for the dependence of both the cluster fractal dimension d_f and the kinetic exponent z on KBr concentration are shown in Figure 3. For ionic strengths above 1 M, both parameters take constant values that are not dependent on salt concentration: $z = 0.60 \pm 0.08$ and $d_f = 1.435 \pm 0.023$. However, a decrease in the KBr concentration below 1 M affects both kinetic and structural properties of the aggregation process. On one hand, exponent z decreases continuously from its maximum value, which means that the aggregation rate goes down and the colloidal system tends to be stable. In the limit of very low ionic strength, the aggregation becomes completely inhibited, and a 2D colloidal crystal is formed. On the other hand, the fractal dimension increases suddenly at 1 M until a value of 1.53 is reached.

These results allow us to define the limiting value 1 M as the CCC for 2D aggregation (i.e., the salt concentration above which the kinetic exponent and fractal dimension reach constant values). This is a very high salt concentration that does not allows double-layer electrostatic repulsion to account for the stability experimental results because of its short-range nature and the fact that it does not change appreciably in the studied interval of KBr concentration from 0.1 to 2 M. So, more long-ranged interaction are needed to justify the colloidal stability at the air−solution interface. These long-range interaction are capable of explaining the decrease in exponent z at low salt concentrations,[18,40] as an increase of the repulsive forces range reduces large-cluster reactivity and, consequently, exponent z. The existence of these interactions can be explained if there are monopoles and/or dipoles in the air-exposed part of the colloidal particles.

The same explanation has already been suggested by Aveyard et al.[16] when comparing theoretical predictions with experimental results for latex particles trapped at the air/water and the octane/water interface at similar electrolyte concentrations. In that work, they did not consider the double-layer repulsion through the water phase. They remarked that the interaction between the residual charges dominates the electrostatic double-layer interaction of the particles through water, which is screened by the electrolyte except at very low ionic strength.

During the spreading of the particle at high ionic strengths ([KBr] > 1 M), the high subphase counterion concentration emphasizes the dipole formation mechanism discussed in section 2. At such a high ionic strength, all dissociated groups of the dispersed particles trap counterions, making impossible the monopole appearance, and only dipoles exist at the air-exposed part of the particles. However, as the salt concentration is reduced below the CCC, the counterion trapping mechanism becomes less effective and, consequently, a certain number of the initially dissociated groups can emerge as monopoles at the air phase. Finally, for extremely low salt concentrations, a lack of counterions allows for a larger number of monopoles, which can stabilize the 2D colloidal system.

Since all KBr concentrations used to induce aggregation in our experiments are high, there are always enough counterions at the subphase, and nearly all dissociated groups form dipoles. Therefore, a very low monopole fraction, f_{mon}, is expected for all of the studied salt concentrations. According to this, we will consider the dipole number to be a constant value independent of the salt concentration; hence, the dipole fraction f_{dip} must be a common constant parameter for all computer simulations. It should be noted that this approximation is valid only for high ionic strengths since, as stated above, a nonnegligible decrease of f_{dip} is expected for very low salt concentrations.

As $f_{mon} \approx 0$ for KBr concentrations above the CCC, there is not a monopolar interaction between the particle emergent parts, and the particles repel each other mainly by dipolar interactions. The long-range character of dipolar interactions prevents the system from reaching the pure diffusion-limited cluster aggregation limit (DLCA). This fact can be demonstrated by comparing the theoretical kinetic exponent $z = 0.712$ at the experimental surface fraction $\varphi = 0.04$[41] with the experimental one $z = 0.60 \pm 0.08$, which is lower, as expected, from the long range of dipolar interactions.

(40) Robinson, D. J.; Earnshaw, J. C. *Phys. Rev. A* **1992**, *46*, 2055.
(41) González, A. E.; Martínez-López, F.; Moncho-Jordá, A.; Hidalgo-Álvarez, R. *J. Colloid Interface Sci.* **2002**, *246*, 227.

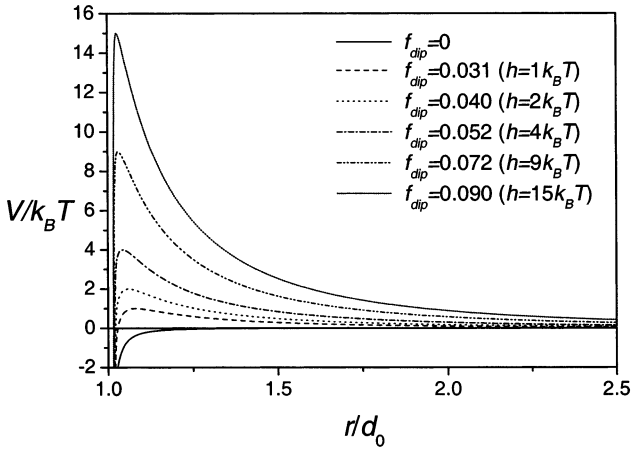

Figure 4. Total interaction energy for particles having dipole fractions from 0 to 0.09; the monopole fraction was chosen to be $f_{mon} = 0$. Both the height (h) and the range of the interaction potential increase with f_{dip}. Distance is normalized by the particle diameter d_0, and energy, by the thermal energy K_BT.

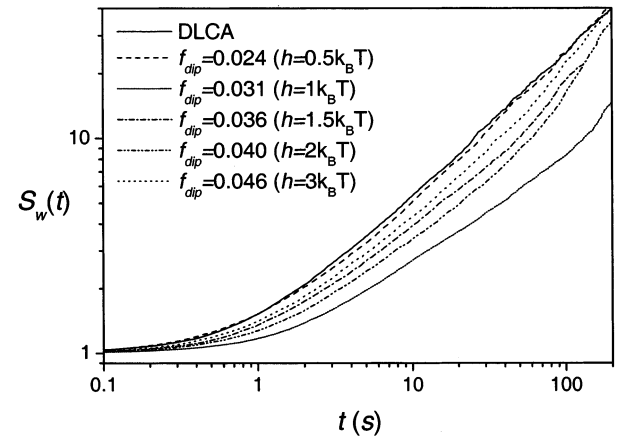

Figure 5. Time dependence of the weight-average cluster size, S_w, obtained from simulations for different f_{dip} values and $f_{mon} = 0$. A pure Brownian aggregation (DLCA regime) has also been included (—) to allow the clear observation of the effects of the long-range dipolar repulsion.

The comparison between experimental and Brownian dynamics simulation results was carried out using two fitting parameters, f_{dip} and f_{mon}. The first parameter, f_{dip}, was obtained by fitting the experimental data d_f and z with the simulation data, for KBr concentrations above the CCC, when $f_{mon} \approx 0$. Once f_{dip} was determined, the experimental results below the CCC were fitted by increasing f_{mon} as the salt concentrations decreased while the dipole fraction was kept constant.

4.1. Fitting for [KBr] > CCC. Figure 4 shows the effect of the dipolar term on the total interaction potential for several dipole fractions, assuming $f_{mon} = 0$. It should be noted that even for a small dipole fraction quite a high barrier—several times the thermal energy—is found. Furthermore, as Figure 4 also shows, both the barrier height and the range of interaction grow for increasing values of f_{dip}.

Simulations for high ionic strengths were carried out at different f_{dip} values. A total number of $N_0 = 10^4$ particles were placed randomly inside a square box whose side length was adequately chosen to achieve the same surface fraction value as the experimental one, $\varphi \approx 0.04$. The time dependence of the weight-average cluster size computed from simulations is shown in Figure 5 for several f_{dip} values. In addition, a DLCA simulation, without interaction, has been included in order to observe clearly the influence of dipolar repulsive interactions on the aggregation kinetics.

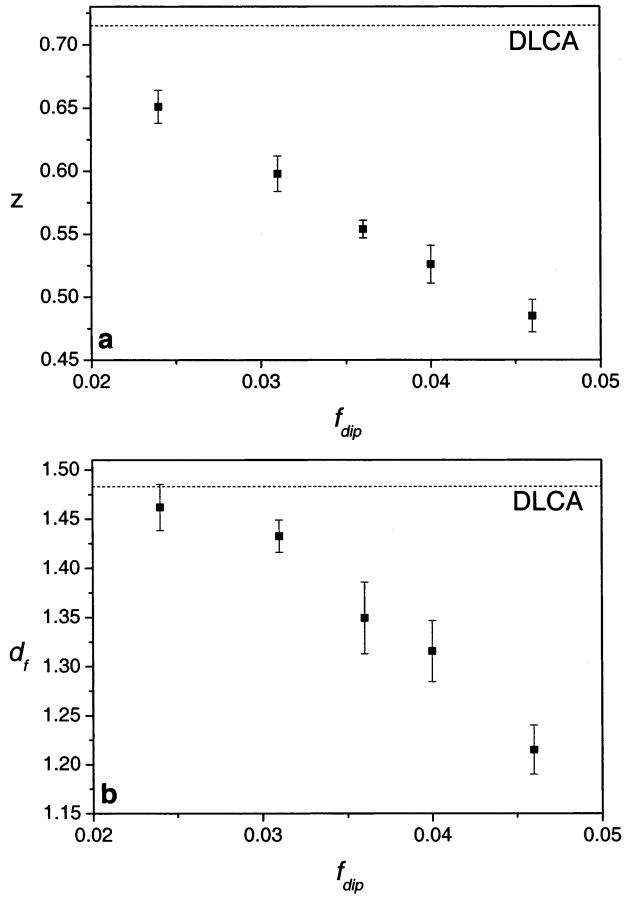

Figure 6. Kinetic exponent z (a) and cluster fractal dimension d_f (b) obtained from simulations as a function of f_{dip}, $f_{mon} = 0$. The corresponding DLCA value is also indicated (- - -).

As the results shown in Figure 5 indicate, the decay of the S_w curve slope for increasing f_{dip} is an immediate consequence of the long-range nature of the dipolar interactions. However, this slope does not remain constant along the overall aggregation process. On the contrary, it grows continuously and tends to the DLCA value for very long times, when large clusters exist on the surface. This effect is a result of the large cluster radius for long aggregation times. When the cluster radius exceeds the repulsive barrier range, both the repulsion felt by these large clusters and their reactivity do not change any more with cluster size, and the kinetic regime approaches the Brownian limit. The time for this crossover increases with the repulsive barrier width and so with the dipole fraction. Disregarding the long-time limit, kinetic exponent z was obtained only in the intermediate scaling region.

Kinetic exponents calculated from the simulated curves, through eq 1, are shown in Figure 6a as a function of the dipole fraction. For the DLCA regime, a value $z = 0.715$ is obtained, in agreement with simulation results found in ref 41. As indicated in section 2, the decrease of z for increasing f_{dip} follows directly from the rise of the repulsive potential range as clusters of any type repel each other more strongly, so the reactivity is lower. As an example, when $f_{dip} = 0.046$, the potential barrier height is $h = 3k_BT$ and $z = 0.485$, whereas $z = 0.712$ for the DLCA regime.

The aggregation kinetic information can be enhanced with the structural information. In this case, the cluster fractal dimension was calculated by applying the radius-

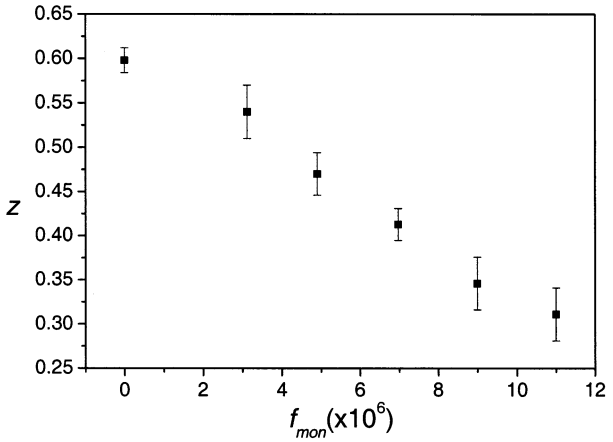

Figure 7. Kinetic exponent z obtained from simulations as a function of f_{mon}. The dipole fraction was consider constant, $f_{dip} = 0.031$.

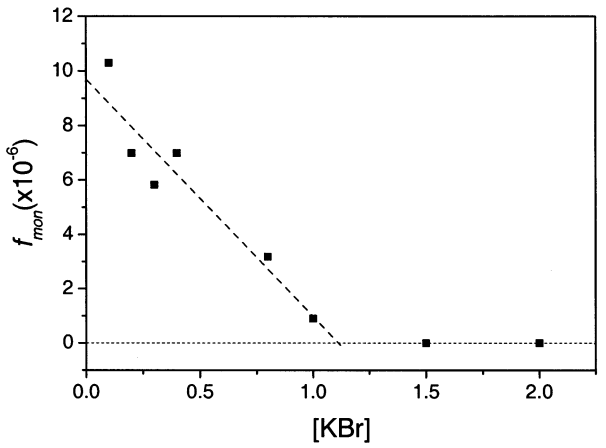

Figure 8. Estimated monopole fraction as a function of the KBr concentration. Below the CCC ([KBr] = 1 M), f_{mon} grows linearly for decreasing KBr concentrations.

of-gyration method to clusters formed during the simulated aggregation. As Figure 6b shows, the fractal dimension decrease with dipole fraction, and the value for noninteracting particles, $d_f = 1.484$, agrees with the fractal dimension value for DLCA at the same particle density.[41] This monotonic decrease is also a consequence of the long-range nature of dipolar forces, and the repulsive interaction increase when the dipole fraction becomes higher. So small fractal dimension values have already been reported by Hurd and Schaefer[8] in 2D colloidal aggregation experiments. As they stated, long-range repulsions encourage aggregation at cluster tips, leading to a decrease of both the cluster compactness and the fractal dimension. In our particular case, simulations show that the fractal dimension decays until $d_f = 1.215$ for $f_{dip} = 0.046$.

As shown in Figure 3, $z = 0.6$ and $d_f = 1.435$ for experiments above the CCC. These experimental values agree very well with those value, $z = 0.598 \pm 0.014$ and $d_f = 1.433 \pm 0.016$, obtained from simulations at $f_{dip} = 0.031$; see Figure 6a and b. Thus, our model is able to explain and to fit experimental results above the CCC using a dipole fraction of $f_{dip} = 0.031$ that leads to a repulsive interaction potential with a barrier height close to the thermal energy ($h \approx k_B T$). Furthermore, this result indicates that the dipole−dipole interaction is able to slow the aggregation process even at large salt concentrations.

As indicated, the dipole fraction is expected to be constant for all performed experiments, so the fitted dipole fraction value, $f_{dip} = 0.031$, will be kept constant for simulations below the CCC.

4.2. Fitting for [KBr] < CCC. For salt concentrations below the CCC, the monopolar interaction (eq 14) must be included in the total interaction potential. Because of the long range of monopole−monopole interactions, particles interact with image particles in all periodic cells, so the computation of the monopolar interaction force is more difficult and time-consuming. Thus, to reduce the computation time, the initial number of particles was reduced to $N_0 = 1000$.

The long-range monopolar Coulombic forces produce such strong stabilization that only a very small monopole fraction is sufficient to impede aggregation and to structure the colloidal system into a triangular lattice. Consequently, the monopole fraction at the particle top, f_{mon}, must be believed to be quite small for all studied KBr concentrations.

By increasing f_{mon}, both the height and range of the repulsive barrier grow. This affects the aggregation kinetics as is shown in Figure 7, where z exponents from simulations are plotted as a function of f_{mon}. It should be pointed out that long-range Coulombic interactions produce a significant continuous decrease of z, even for such small monopole fractions. Indeed, z changes from 0.598 ± 0.014 to 0.31 ± 0.03 when f_{mon} goes from 0 to 1.1×10^{-5}.

Values in Figure 7 can be interpolated to estimate monopole fractions that correspond to z exponents obtained at each experimental KBr concentration below the CCC. Results from this interpolation indicate that $f_{mon} \approx 1.03 \times 10^{-5}$ for [KBr]= 0.1 M and decreases to zero for salt concentrations near 1 M (see Figure 8). Also, the decay of f_{mon} with salt concentration seems to follow a linear dependence. However, until now, there was not a theoretical model for this dependence, and the dashed, straight line must be considered to guide the eye. In any case, this curve resembles that corresponding to the stability factor (W in 3D colloidal aggregation experiments).

Recent papers reported larger values for f_{mon}: Aveyard et al.[16] found a monopole fraction of about 1% of the total charge, and Sun and Stirner[23] obtained a value close to 0.4% for latex particles trapped at the octane/water interface. In such systems, particles remain, forming highly ordered structures due to monopolar interaction, which was found to be quite insensitive to the electrolyte concentration. However, at the air/water interface, they found that a relatively high salt concentration is able to damp out the Coulombic repulsion leading to spontaneous coagulation. This experimental result has two important consequences: (i) Since particles at the air/water interface can coagulate, a lower value of f_{mon} is expected here. (ii) f_{mon} is sensitive to the subphase salt concentration at the air/water interface, and for a large enough ionic strength, it will approach zero. Both conclusions agree with our experimental results and the f_{mon} dependence shown in Figure 8.

It should be noted that values obtained for the monopole fraction at the air/latex interface are very small as compared with dipole fraction, which is the maximum number of monopoles lower than 0.04% of the dipole number. This justifies our assumption that f_{dip} is a constant parameter for all studied KBr concentrations.

Since f_{dip} does not changes, f_{mon} is the parameter controlling colloidal stability at the air−water interface. In addition, the 2D critical coagulation concentration may be characterized as the salt concentration at which $f_{mon} = 0$:

$$\mathrm{CCC} = [\cdot]_{f_{mon}=0} \tag{22}$$

This theoretical result also explains the experimental behavior of the CCC with the counterion valence:[18] CCC-(v) $\approx 1/v$. Indeed, if counterions from the solvent are doubly charged, then it will be necessary for half of the salt concentration to balance the dissociated groups of the spread particles, and so the CCC is reduced by half.

The statistical limitations, derived from the small number of initial particles in the last set of simulations, forbid us to calculate the cluster fractal dimension, d_f, which is defined in the large-cluster size limit. Although the exact value of d_f is unknown, it is expected that it decreases for increasing f_{mon} (i.e., for decreasing salt concentrations) because cluster−cluster coagulations tend to occur at the external tips of their structures. However, such expected behavior is contrary to our experimental observations (see Figure 3b) and to those by other authors.[29] This fact points out that cluster structure at low subphase ionic strength is not determined only by cluster Brownian motion and repulsive interactions. Thus, new effects that have not been considered in the above-described theoretical model must be taken into account. Moreover, the sudden change from $d_f \approx 1.44$ to $d_f \approx 1.54$ at [KBr] = 1 M = CCC cannot be explained in terms of a continuous change in the width and height of the repulsive barrier.

A plausible explanation for this argument is particle restructuration inside the clusters, which can occur if particles aggregate in a secondary minimum instead of a primary one. Another plausible explanation is the existence of an attractive potential well in the interaction potential for low salt concentration.[42,43,44] Unfortunately, it must be remarked that our potential model does not allow for such a secondary minimum or for an attractive potential well.

Nonetheless, the aggregation kinetic properties as the z exponent are affected only weakly by the existence of a secondary minimum since the long-range interactions play the most important role in the cluster lifetime. In other words, the kinetic aspects are characterized by the average time that the clusters spend while they are moving at the interface before coagulating. Since for low salt concentrations this time is mainly determined by the monopolar long-range repulsive interactions, the above-described model will offer a good theoretical description for the kinetic behavior, as becomes clear in these results and from those in a previous work for the same experimental system.[18] Moreover, the model accounts for the experimental results in stable colloidal monolayers, where a very long-range pair interaction potential between colloidal particles at the air-distilled water interface (without adding any electrolyte) was obtained by means of the inversion of structural data.[17]

5. Conclusions

The DLVO theory is not capable of explaining experimental data from colloidal aggregation at the air−water solution interface. As the experimental results show, particles at this interface are very stable, and new long-range repulsive interaction must be included to explain the data for high electrolyte concentrations. So, our model also includes dipolar and monopolar interactions between the emergent parts of the particles, which depend on dipole and monopole fractions, f_{dip} and f_{mon}, at the air-exposed part of the particles.

Simulations carried out to fit the proposed potential model to the experimental data indicate that for higher KBr concentrations only dipolar interactions exist and the interaction potential has a repulsive barrier with a height of about k_BT. However, for KBr concentrations below the CCC, monopolar Coulomb repulsive interactions must be taken into account. Thus, CCC can be featured as the salt concentration at which the monopole fraction becomes zero.

As the comparison between the experimental data and simulation suggests, the most important parameter controlling the aggregation of charged colloidal particles at the air−water solution interface is the range particle−particle interaction. Thus, the decay of the exponent z with decreasing KBr concentrations can be explained only in terms of an increase in the range of interaction, that is, an increase in the dipole fraction at the air-exposed part of the particle.

Although the proposed theoretical model also accounts for the fractal dimension at high KBr concentrations, it fails when applied to the description of the fractal dimension of clusters formed at low salt concentrations. A restructuring mechanism can explain the observed high fractal dimension values.

Acknowledgment. A.M.J, F.M.L., and R.H.A. thank the Ministerio de Ciencia y Tecnología, Plan Nacional de Investigación Cientıfica, Desarrollo e Innovación Tecnológica (I+D+I), MAT 2000-1550-C03-01 for financial support. A.E.G. was partially supported by CONACYT, Mexico (grant no. 34343-E) and extends his gratitude to the Supercomputing Committee at UNAM for the generous amount of supercomputing time granted.

LA0258805

(42) Guezzi, F.; Earnshaw, J. C. *J. Phys.: Condens. Matter* **1997**, *9*, L517.

(43) Ruiz-Garcıa, J.; Gámez-Corrales, R.; Ivlev, B. I. *Phys. Rev E* **1998**, *58*, 660.

(44) Stamou, D.; Duschl, C.; Johannsmann, D. *Phys. Rev E* **2000**, *62*, 5263.